Cell Reports
Physical Science

CellPress
OPEN ACCESS

Article

Thalidomide derivatives degrade BCL-2 by reprogramming the binding surface of CRBN

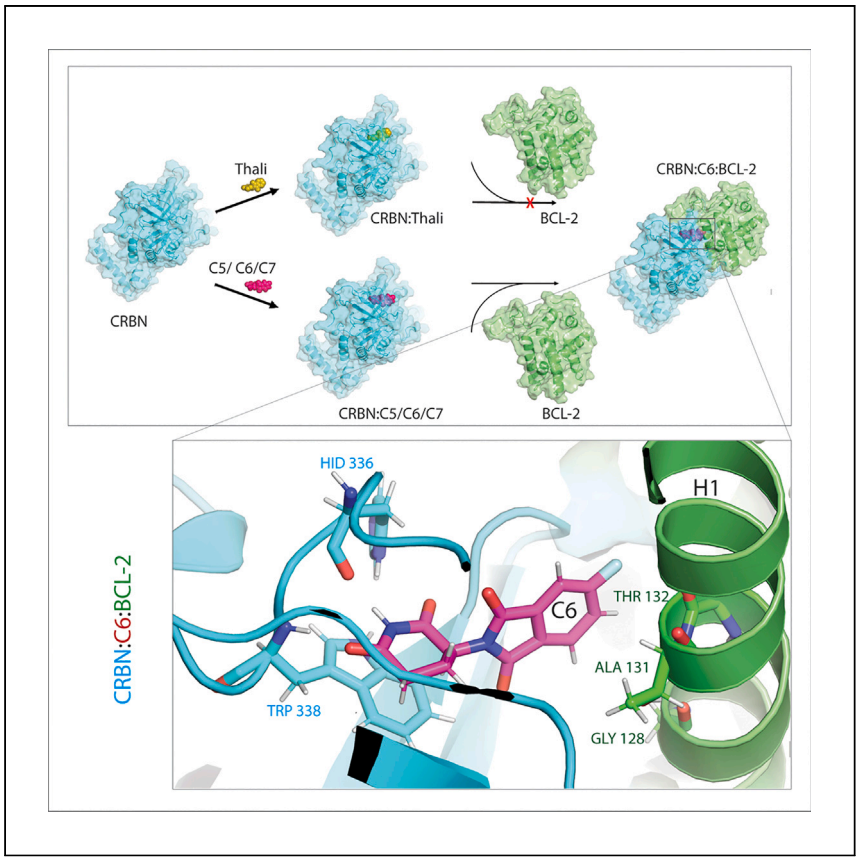

Leveraging the transformative potential of thalidomide derivatives, Wang et al. unveil BCL-2 protein degraders. Through proteomics and AlphaFold modeling, this work identifies key interactions enabling the targeting of venetoclax-resistant mutations, offering new therapeutic avenues and enhanced survival prospects in cancer models.

Jianhui Wang (王建辉), Marcel Heinz, Kang Han (韩康), ..., Jun Zhou (周俊), Ivan Dikic, Xinlai Cheng (承辛来)

cheng@pharmchem.uni-frankfurt.de

Highlights

Thalidomide derivatives are identified as BCL-2 degraders

AlphaFold predicts GLY128, ALA131, and THR132 are key in the binding

Derivatives degrade venetoclax-resistant BCL-2 mutations

Survival is boosted in *Drosophila* tumor model

Wang et al., Cell Reports Physical Science 5, 101960
May 15, 2024
https://doi.org/10.1016/j.xcrp.2024.101960

Cell Reports
Physical Science

CellPress
OPEN ACCESS

Article

Thalidomide derivatives degrade BCL-2 by reprogramming the binding surface of CRBN

Jianhui Wang (王建辉),[1,2] Marcel Heinz,[3] Kang Han (韩康),[4] Varun J. Shah,[5] Sebastian Hasselbeck,[1,2] Martin P. Schwalm,[1,2,8,9] Rajeshwari Rathore,[5] Gerhard Hummer,[3,6] Jun Zhou (周俊),[4] Ivan Dikic,[5] and Xinlai Cheng (承辛来)[1,2,7,9,10,11,*]

SUMMARY

Recent studies demonstrate that modified thalidomide chemically alters the binding surface of its binding E3 ligase, CRBN, leading to the degradation of new substrate proteins. In this study, we conduct a proteome-wide analysis of thalidomide-like compounds and pinpoint three derivatives (C5, C6, and C7) that specifically target and degrade the BCL-2 protein. Using AlphaFold-driven molecular modeling combined with experimental data, we suggest that GLY128, ALA131, and THR132 are crucial in forming a CRBN-C5-BCL-2 ternary complex. This interaction is notably distinct from that of venetoclax, a known clinical BCL-2 inhibitor that interacts with the BH3 domain. Significantly, these thalidomide derivatives have the ability to degrade BCL-2 mutations that are resistant to venetoclax, thereby enhancing survival rates in a Notch-depleted *Drosophila* intestinal tumor model. Our findings highlight the critical role of targeted modifications to the E3 ligase surface in altering its binding affinity and achieving a new substrate protein profile.

INTRODUCTION

BCL-2 is the prototype of the BCL-2 family, which includes both anti-apoptotic proteins (e.g., BCL-2 and BCL-XL) and pro-apoptotic proteins (e.g., BAD and BAX).[1] Its abundant expression in various cancer cell types is closely associated with increased tumor refractoriness and high relapse rates.[2] BCL-2 contains four BCL-2 homology domains (BH1-4). The BH1, BH2, and BH3 domains primarily facilitate dimerization with other BCL-2 family members containing the BH4 domain. This interaction is crucial in preventing mitochondrial outer membrane permeabilization, thereby enabling cancer cells to evade apoptosis, a hallmark of cancer development.[1]

Despite earlier challenges in targeting BCL-2 due to its large and flat interaction domain, which was once deemed unsuitable for small-molecule inhibitors, it has now become a viable chemotherapeutic target.[3,4] Advances in drug discovery technologies, such as fragment-based screening and NMR-based structure-activity relationship studies, have led to the development of several BCL-2 inhibitors. These include BH3 mimetics such as ABT-737 and its orally active derivative, venetoclax (ABT-199), the first-in-class drug manipulating cellular apoptotic machinery.[5] These inhibitors specifically bind to the hydrophobic groove of BCL-2, exhibiting unique binding patterns and setting the stage for further chemical modulators such as WEHI-539.[3,6] However, resistance to these drugs, particularly venetoclax, has been observed in chronic lymphocytic leukemia patients, often due to mutations in the BH3 binding pocket of BCL-2, such as G101V and F104C.[7,8] Therefore,

[1]Buchmann Institute for Molecular Life Sciences, Goethe University, Frankfurt am Main, Germany

[2]Institute of Pharmaceutical Chemistry, Goethe University, Frankfurt am Main, Germany

[3]Max Planck Institute of Biophysics, Frankfurt am Main, Germany

[4]Hunan Key Laboratory of Animal Models and Molecular Medicine, School of Biomedical Sciences, Hunan University, Hunan, China

[5]Institute of Biochemistry II, Goethe University, Frankfurt am Main, Germany

[6]Institute of Biophysics, Goethe University, Frankfurt am Main, Germany

[7]Frankfurt Cancer Institute (FCI), Goethe University, Frankfurt am Main, Germany

[8]Structural Genomics Consortium (SGC), Goethe University, Frankfurt am Main, Germany

[9]German Cancer Consortium (DKTK)/German Cancer Research Center (DKFZ), DKTK Site, Frankfurt-Mainz, Germany

[10]Twitter: @XinlaiC

[11]Lead contact

*Correspondence: cheng@pharmchem.uni-frankfurt.de

https://doi.org/10.1016/j.xcrp.2024.101960

developing new molecules that can target these venetoclax-resistant BCL-2 mutations is of critical importance.[7,8]

The discovery of thalidomide and its derivatives as molecular glue degraders (MGDs) marks a pioneering advancement in drug research. It opens new pathways for targeting proteins, including transcription factors, previously considered undruggable.[9–11] This breakthrough has also catalyzed the development of proteolysis-targeting chimera (PROTAC), a class of heterobifunctional molecules designed for targeted protein degradation.[12–14] Thalidomide and its derivatives function by binding to the cereblon (CRBN) E3 ligase, inducing surface alterations that facilitate interactions with substrate proteins, leading to their degradation. The chemical structures of MGDs not only enhance the precision of targeting proteins, such as C2H2 zinc finger (C2H2 ZF) transcription factors, but also allow for the creation of unique degradation targets.[9–11,15–18] For instance, avadomide and iberdomide specifically degrade ZKSC5 and IKFZ2/4, respectively,[15] while lenalidomide targets CK1.[16]

Recent studies highlighting the effectiveness of VHL- and CRBN-based PROTACs in degrading BCL-2 family proteins[19–21] inspired our investigation into whether thalidomide derivatives could similarly target these proteins. Our extensive proteome-wide screening of approximately 30 thalidomide-related compounds led to the identification of three thalidomide analogs (C5, C6, and C7) capable of degrading both BCL-2^{WT} and its venetoclax-resistant variants (BCL-2^{G101V} and BCL-2^{F104C}) in leukemia cells. Our study, integrating AlphaFold-driven molecular modeling with experimental data, revealed that C5 interacts with GLY128, ALA131, and THR132, in proximity to the BH1 domain of BCL-2, for its degradation. Notably, C5 also showed potential in enhancing survival in *Drosophila* intestinal tumor models caused by Notch depletion, suggesting a promising avenue for treating venetoclax-resistant tumors.

RESULTS

Proteome-wide screening for thalidomide analogs targeting BCL-2

Recent studies by Pal et al., Lv et al., and Wang et al. have independently demonstrated the degradation of BCL-2 using both CRBN- and VHL-based PROTACs,[19–21] suggesting the formation of CRBN/VHL-PROTAC-BCL2 ternary complexes crucial for ubiquitin transfer during degradation. Particularly, the molecular modeling study conducted by Lv et al. implied a direct interaction between BCL-2 and the E3 ligase in the presence of a PROTAC containing a short C-space linker (Figure S1A).[20] This resembles the molecular glue-mediated degradation process, where an intrinsic affinity between CRBN/VHL and BCL-2 in the absence of the ligand is crucial, even without a ligand present.[22,23]

In our search for thalidomide-like compounds that could degrade BCL-2 family proteins via CRBN recruitment, we analyzed the entire proteome in cells treated with various thalidomide analogs. We discovered that C5, C6, or C7 (10 μM, 6 h, structures in Figure S1B) effectively reduced BCL-2 expression in Jurkat cells without impacting other BCL-2 family members (Figures 1A, 1B, and S1C).

In agreement with previous reports,[18] thalidomide showed minimal impact on protein expression in our experimental setup (fold changes >1.5, $p < 0.05$, Figure 1A). By contrast, we observed the downregulation of certain C2H2 ZF transcription factors, such as ZFP91, ZNF98, and IKZF3, in the presence of pomalidomide (Figure 1A).

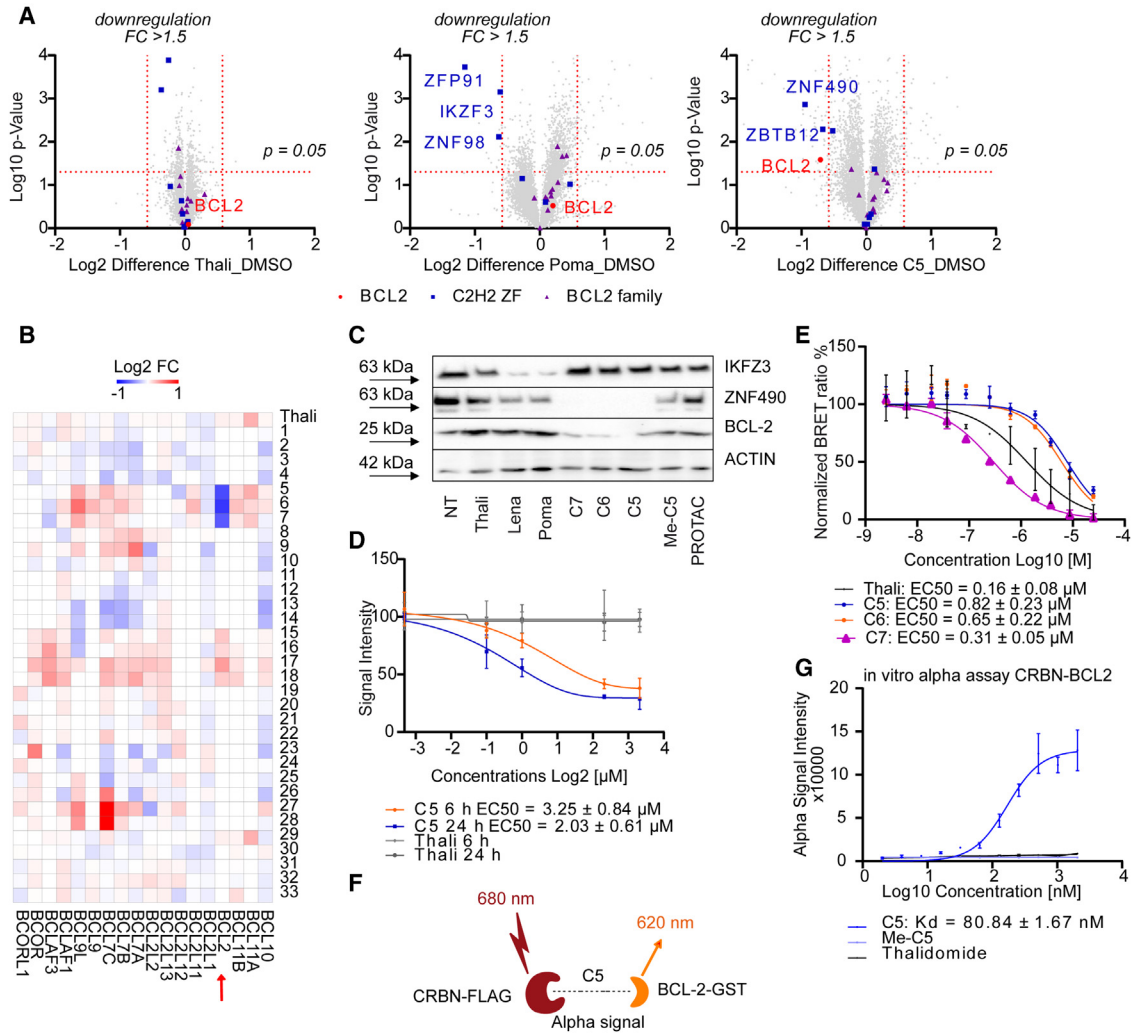

Figure 1. Proteome-wide screening for thalidomide-analogs targeting BCL-2

(A) Proteomic analysis of 10 μM thalidomide-, pomalidomide- (poma), or C5-treated Jurkat cells (6 h). Red, BCL-2; blue, selective C2H2 zinc finger transcription factor; lilac, other proteins of BCL-2 family. Threshold: $p < 0.05$; fold-change (FC) of downregulation <1.5. Average values from three independent experiments ($n = 3$).

(B) Heatmap of the expression levels of BCL-2 family proteins in cancer cells treated with thalidomide (thali) or thalidomide-like compounds (10 μM, 6 h) in a proteome-wide screening.

(C) Comparison of the efficiency of BCL-2, ZNF490, and IKFZ3 degradation in THP-1 cells treated with 10 μM of thalidomide, lenalidomide (lena), poma, C5, C6, C7, methylated C5 (Me-C5), or BCL-2 PROTAC for 18 h.

(D) Comparison of the efficiency of BCL-2 degradation in THP-1 cells treated with C5 or thali ($n = 3$).

(E) Comparison of EC_{50} values of thalidomide, C5, C6, and C7 binding to CRBN in cell-based BRET assay ($n = 3$).

(F) Illustration of *in vitro* alpha assay.

(G) Determination of ternary complex formation involving CRBN-FLAG, C5, and BCL-2-GST using *in vitro* alpha assay. Thalidomide and Me-C5 were used as negative controls ($n = 3$). All raw immunoblotting images can be found in Figure S7. Data are represented as mean ± SEM. See also Figures S1 and S2.

Modifications on the phthaloyl-ring (C5, C6, and C7) led to alterations in target protein profiles, including new zinc finger proteins (ZNF490, ZNF580, and ZBTB12)[15,18] and BCL-2 (Figures 1A, 1B, and S1C), suggesting the dependence of substrate profiles on the chemical structures of degraders.[15,18]

Next, we compared BCL-2 expression in Jurkat cells treated with 10 μM of thalidomide or its derivatives. Given that the -NH group on the glutarimide motif is

indispensable for thalidomide binding to CRBN,[9] we introduced a methyl group at this position in C5 (Me-C5), serving as a negative control (Figure S1B, indicated in red, the chemical characterization can be found in Figure S8). For comparison, we also included a commercial BCL-2 PROTAC by Wang et al. This PROTAC conjugating acenaphtho[1,2-b]pyrrole, a BH3 mimetic, into thalidomide, effectively degraded BCL-2 in HeLa cells.[21] Our immunoblotting results (Figures 1C and S1D) confirmed that C5, C6, and C7, but not thalidomide, lenalidomide, pomalidomide, or Me-C5, effectively reduced BCL-2 expression. As reported previously, a notable decrease in IKZF3 levels was also observed with pomalidomide or lenalidomide treatments (Figures 1C and S1D).[15] In addition, a slight reduction in BCL-2 levels (~20%) was found with 5 μM of BCL-2 PROTAC (Figures 1C, S1D, and S1E), suggesting a more effective degradation by molecular glue BCL-2 degrader in our test conditions compared with BCL-2 PROTAC. Moreover, qPCR results showed a slight increase in BCL-2 transcription, indicating a possible negative feedback mechanism in response to C5-mediated BCL-2 degradation (Figure S1F).

Furthermore, C5, C6, and C7 effectively reduced BCL-2 expression in both Jurkat and THP-1 cells (Figures 1D and S2A–S2J) and this reduction persisted for at least 8 h even after the removal of C5 (Figure S2L). By contrast, BCL-2 remained unaffected in the presence of thalidomide (Figures 1D, S2A, S2C, S2D, S2G, S2I, and S2J). Importantly, other members of the BCL-2 family, such as BCL-XL, BAD, and BAX, remained unchanged in response to C5 at concentrations up to 20 μM for 24 h (Figure S2K).

Using the cellular CRBN-NanoBRET assay, we observed that C5, C6, and C7 exhibited a lower binding affinity to CRBN compared with thalidomide itself (Figure 1E), suggesting that binding affinity might not be the primary determinant in recruiting new substrates. *In vitro* experiments revealed the formation of a ternary complex involving CRBN, C5, and BCL-2, as demonstrated by alpha bead assays (K_d ~80 nM). Notably, no alpha signal was detected in the presence of either thalidomide or Me-C5 (Figures 1F and 1G). This suggests that the chemical modifications in C5, C6, and C7 may alter the surface of CRBN upon binding, facilitating the ternary complex formation with BCL-2.

It is important to note the distinct conditions of the *in vitro* and cellular assays. For the *in vitro* alpha assay, we used commercially available CRBN-FLAG and BCL-2-GST proteins, and the reaction occurred in alphaLISA protein-protein binding buffer. In contrast, for the NanoBRET assay, HEK293T cells were transfected with CRBN-NanoLuc fusion and DDB1-FuGENE HD plasmids. The significant differences in the efficacy of the compounds observed in the cellular NanoBRET assay, which was about 10-fold lower than *in vitro*, could be attributed to the use of different assay environments. Factors such as biotransformation, bioavailability, and other microenvironmental influences may also play a substantial role in this variance.

C5-mediated BCL-2 degradation is CRBN dependent

Thalidomide and its derivatives recruit the CRBN E3 ligase to degrade target proteins via the proteasome pathway, in which neddylation plays an important role.[12,13,24] In our study, we observed that both the proteasome inhibitor MG132 and the neddylation inhibitor MLN4924 effectively rescued the C5-induced BCL-2 degradation (Figures 2A and S3A). To further understand this process, we performed immunoprecipitation of BCL-2 followed by immunoblotting using a specific ubiquitin antibody. Our results indicated that increased ubiquitin polymerization on BCL-2 was involved in C5-induced degradation (Figure 2B). Moreover, we noted that

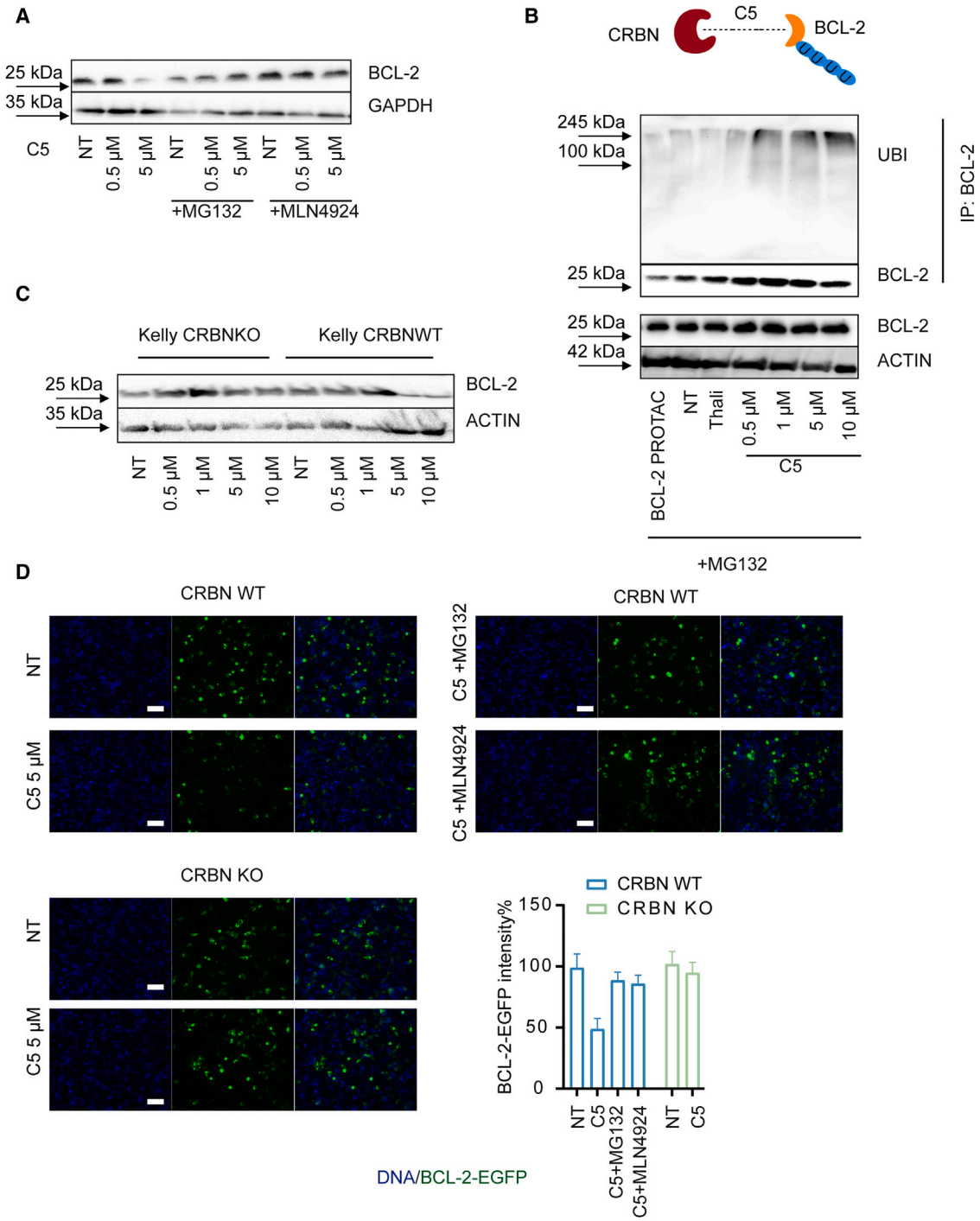

Figure 2. C5-mediated BCL-2 degradation is CRBN dependent

(A) Proteasome inhibitor (MG132) and NEDD8-activating enzyme inhibitor (MLN4924) rescued C5-induced BCL-2 degradation. THP-1 cells were treated with increasing concentrations of C5 in the presence or absence of MG132 (5 μM) or MLN4924 (5 μM) for 6 h.

(B) C5-mediated polyubiquitination was observed on ubiquitin co-precipitated with BCL-2. HEK293T cells were transfected with BCL-2 and treated with C5 and MG132 (5 μM) for 6 h. BCL-2 was used as input control and actin was used as loading control.

(C) C5-mediated BCL-2 degradation was prevented in Kelly CRBN^{KO} cells detected by immunoblotting (6 h).

(D) C5 reduced BCL-2-EGFP in Kelly CRBN^{WT} cells, which was not affected in CRBNKO cells (6 h). Upper left: CRBN^{WT} cells treated with DMSO (0.05%) as control or C5 (5 μM); upper right: CRBN^{WT} cells treated with C5 in combination with MG132 (5 μM) or MLN4924 (10 μM); lower left: CRBN^{KO} cells treated with DMSO or C5; lower right: quantified fluorescence signal intensity. Scale bars, 40 μm. All raw immunoblotting images can be found in Figure S7. See also Figure S3.

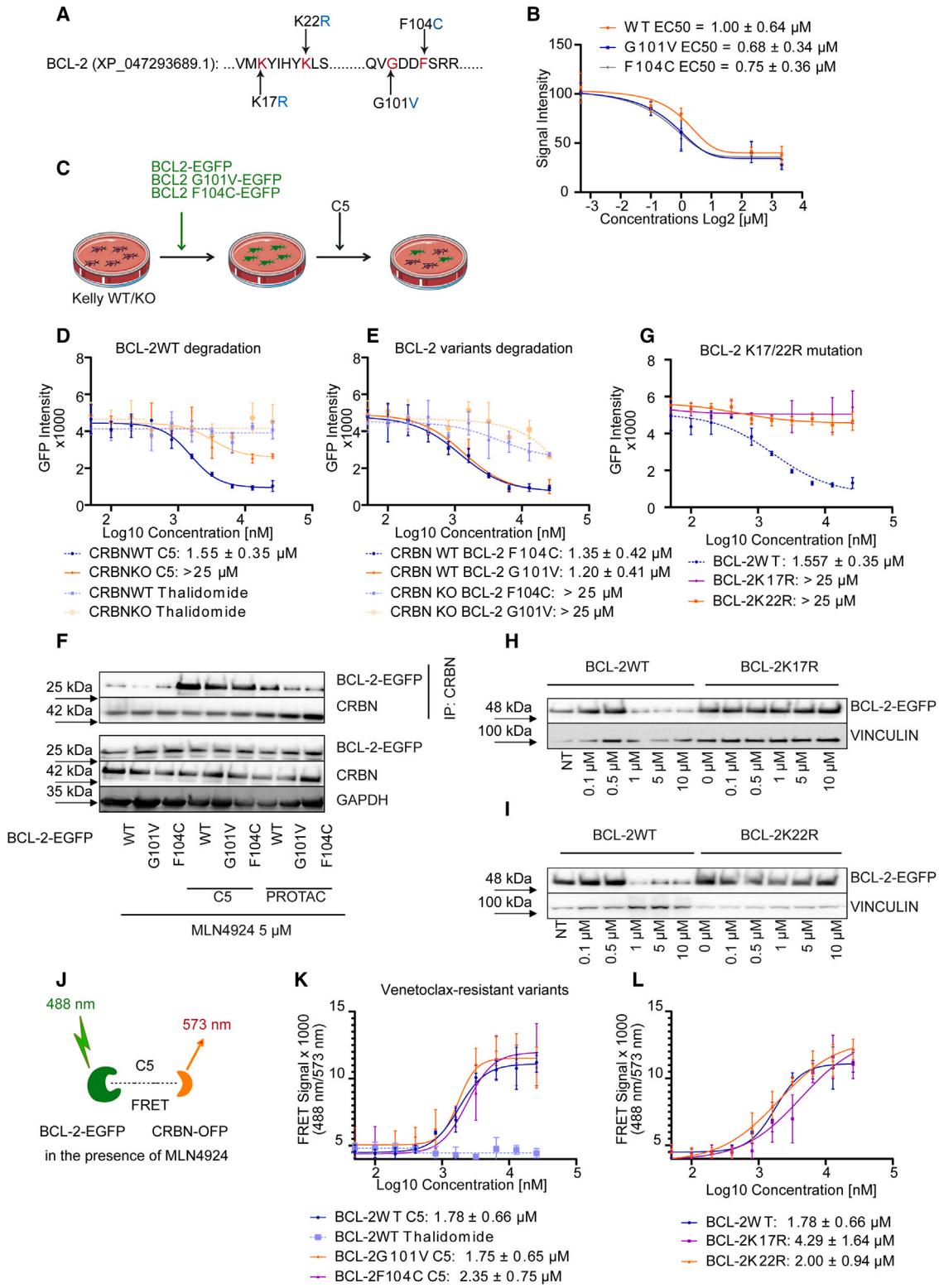

Figure 3. C5 degrades venetoclax-resistant BCL-2^{G101V} and BCL-2^{F104C}

(A) Illustration of K17R, K22R, G101V, and F104C mutations on BCL-2.

(B) Comparison of C5-mediated BCL-2^{WT}, BCL-2^{G101V}, and BCL-2^{F104C} degradation efficiency based on the results of immunoblotting (n = 3).

Figure 3. *Continued*

(C) Illustration of generation of BCL-2-EGFP report cells and treatment.

(D) Comparison of GFP signal intensity in Kelly $CRBN^{WT}$ and $CRBN^{KO}$ cells expressing $BCL\text{-}2^{WT}$-EGFP treated with C5 overnight (n = 3).

(E) Comparison of GFP signal intensity in Kelly $CRBN^{WT}$ and $CRBN^{KO}$ cells expressing $BCL\text{-}2^{G101V}$-EGFP and $BCL\text{-}2^{F104C}$-EGFP treated with C5 overnight (n = 3).

(F) C5-mediated interaction between CRBN and BCL-2 variants. HEK293 cells were transfected with $BCL\text{-}2^{WT}$-EGCP, $BCL\text{-}2^{G101V}$-EGFP, or $BCL\text{-}2^{F104C}$-EGFP and treated with C5 in the presence of MLN4924 (5 μM). CRBN antibody was used for immunoprecipitation. BCL-2 PROTAC was used as a reference.

(G) Comparison of GFP signal intensity in Kelly $CRBN^{WT}$ and $CRBN^{KO}$ cells expressing $BCL\text{-}2^{K17R}$-EGFP and $BCL\text{-}2^{K22R}$-EGFP treated with C5.

(H) Comparison of expression levels of $BCL\text{-}2^{WT}$ and $BCL\text{-}2^{K17R}$ upon treatment of C5 detected by immunoblotting with GFP antibody.

(I) Comparison of expression levels of $BCL\text{-}2^{WT}$ and $BCL\text{-}2^{K22R}$ upon treatment of C5 detected by immunoblotting with GFP antibody. HEK293T cells were transfected with BCL-2WT, $BCL\text{-}2^{K17R}$, or $BCL\text{-}2^{K22R}$ and treated with C5 at indicated concentrations for 6 h.

(J) Illustration of FRET assay based on EGFP-OFP pair. MLN4924 (5 μM) was used to block the degradation.

(K) Comparison of FRET signal intensity in HEK293T cells expressing $BCL\text{-}2^{WT}$, $BCL\text{-}2^{G101V}$, or $BCL\text{-}2^{F104C}$ treated with C5 (n = 3).

(L) Comparison of FRET signal intensity in HEK293T cells expressing $BCL\text{-}2^{WT}$, $BCL\text{-}2^{K17R}$, or $BCL\text{-}2^{K22R}$ treated with C5 (n = 3). All raw immunoblotting images can be found in Figure S7. Data are represented as mean ± SEM. See also Figure S4.

the reduction in BCL-2 protein levels occurred only in Kelly $CRBN^{WT}$ but not in Kelly $CRBN^{KO}$ cells (Figures 2C and S3B).[18] This was further substantiated by overexpressing BCL-2-EGFP in both cell lines and observing the changes under a fluorescence microscope. The results clearly showed a reduction in green fluorescence intensity only in the C5-treated Kelly $CRBN^{WT}$ cells (Figure 2D). This finding implicates that the C5-mediated BCL-2 degradation is CRBN und ubiquitin-proteasome dependent.

C5 degrades venetoclax-resistant $BCL\text{-}2^{G101V}$ and $BCL\text{-}2^{F104C}$

The acquisition of the G101V mutation in BCL-2 has been identified as the primary cause of rapidly developing refractory disease in up to 50% of patients with hematological malignancies in clinical studies.[7,8] Similarly, the F104C mutation, located in the BH3-binding groove of BCL-2, has been shown to confer a 250-fold higher resistance to venetoclax compared with the G101V mutation.[8] To determine the degradation capability of C5 on these BCL-2 variants, we engineered point mutations G101V and F104C (Figure 3A) and overexpressed $BCL\text{-}2^{G101V}$-EGFP and $BCL\text{-}2^{F104C}$-EGFP in Kelly cells. Our immunoblotting results showed that C5 effectively degraded both mutant proteins with similar EC_{50} values (~1 μM) as observed with the wild-type protein (Figures 3B and S4A). As expected, the degradation effects were reversed by MG132 (Figure S4B).[25] Furthermore, a concentration-dependent reduction in green fluorescence signal intensity was observed in $CRBN^{WT}$ cells expressing $BCL\text{-}2^{WT}$-EGFP, $BCL\text{-}2^{G101V}$-EGFP, and $BCL\text{-}2^{F104C}$-EGFP when treated with C5 (Figures 3C–3E). Consistent with our previous results, no significant signal alteration was detected in cells expressing $CRBN^{KO}$ or those treated with thalidomide (Figures 3C–3E and S4C).

Co-immunoprecipitation experiments involving CRBN and BCL-2 in cells expressing these BCL-2 variants, conducted in the presence of MLN4924, revealed a clear C5-induced interaction of $BCL\text{-}2^{WT}$-EGFP, $BCL\text{-}2^{G101V}$-EGFP, and $BCL\text{-}2^{F104C}$-EGFP with CRBN (Figure 3F). This interaction was notably weaker between $BCL\text{-}2\text{-}EGFP^{WT}$ and CRBN when BCL-2 PROTAC was used. Furthermore, the interaction almost disappeared for $BCL\text{-}2^{G101V}$-EGFP or $BCL\text{-}2^{F104C}$ (Figure 3F), indicating that C5 is a more effective degrader of BCL-2, regardless of the presence of BH3 domain mutations, compared with BCL-2 PROTAC (Figure S4D).

Our above findings indicate that C5-mediated BCL-2 degradation is reliant on the ubiquitin-proteasome pathway. The lysine residues K17 and K22 are highly conserved across BCL-2 variants.[26] Previous studies have demonstrated the critical

role of K17 in BCL-2 ubiquitination and degradation (Figure 3A).[20,26] To explore the specific function of K17 and K22 in C5-mediated BCL-2 degradation, we introduced mutations K17R and K22R. We observed that both these mutations effectively prevented C5-mediated degradation in Kelly CRBN^{WT} cells (Figure 3G), which was further confirmed by immunoblotting analyses of cells expressing either BCL-2^{K17R} (Figure 3H) or BCL-2^{K22R} (Figure 3I). In addition, the analysis of EGFP intensity provided further evidence to support that C5 effectively repressed the expression of G101V and F104V variants, as demonstrated by a remarkable decrease in the fluorescence levels, while no notable reduction was observed in cells expressing BCL-2^{K17R} or BCL-2^{K22R} (Figure S4E), suggesting the involvement of both lysine residues in the degradation process mediated by C5.

We adapted our previously established EGFP-OPF fluorescence resonance energy transfer (FRET) system[12] to investigate the cellular interaction between BCL-2 and CRBN in HEK293 cells expressing BCL-2-EGFP and CRBN-OFP (Figure 3J) in the presence of MLN4924 (5 μM).[12] We observed an FRET signal in cells expressing BCL-2^{WT}, BCL-2^{G101V}, or BCL-2^{F104C}, and treated with C5, indicating the ternary complex formation. As expected, no signal was detectable in the presence of thalidomide (Figure 3K). Interestingly, FRET signals were also detectable in cells expressing BCL-2^{K17R} or BCL-2^{K22R}, suggesting that the mutations K17R or K22R did not affect the binding interface of BCL-2 to C5 (Figure 3L).

G128, A131, and T132 are essential for BCL-2 degradation

We further gained structural and dynamic information of the ternary complex through *in silico* modeling and simulations of the C5- and C6-mediated BCL-2:CRBN complexes.

Eight initial ternary complex models were constructed based on BCL-2:CRBN docking and glue docking to BCL-2 (Figures 4A and S5A). Ternary complex structures and dynamics were explored in 1 μs MD simulations for each model and revealed reorientations of BCL-2 from the initial complex structures (Figure 4A, C6.1). The Cα RMSDs of BCL-2 range from 5 to 25 Å and plateau mostly during the rest of the simulations, indicating moderately stable complex structures in different states. The solvent-inaccessible surface area (Figure S5B) of BCL-2 in the ternary complexes also indicates moderately stable ternary complexes as the surface sizes plateau after initial reorientations of the target protein at the CRBN binding site (Figure 4A). Larger fluctuations in Figure S5A compared with the Cα RMSD are due to the flexible loop region in BCL-2, which is not considered in the RMSD calculations. The observed BCL-2 reorientations at the beginning of the simulations indicate that the initial protein:protein complex structures obtained by docking relax to energetically more favorable conformations during the MD simulations.

Three ternary complex models show lysine accessibility to ubiquitination in static E3 ligase complexes. Four E3 ligase complexes with different DDB1 orientations were constructed,[27,28] containing CRBN, DDB1, Cullin-1, UBE2D2, NEDD8, RBX1, and "Ub." The eight simulated BCL-2:C6:CRBN complexes were aligned onto the static E3 ligase complexes at the CRBN (Figure 4B). BCL-2 lysine accessibility to ubiquitin in the complex was determined through proximity of LYS17 (BCL-2) to GLY78 (Ub) (Figure 4C). Ternary complex models 1, 6, and 8 were chosen for further investigations and simulations were extended from 1.0 to 5.0 μs.

Different 3-fluoro-phthalimide (C5) and 4-fluoro-phthalimide (C6) orientations of the glues were simulated and showed similar behavior. The phthalimide ring maintained

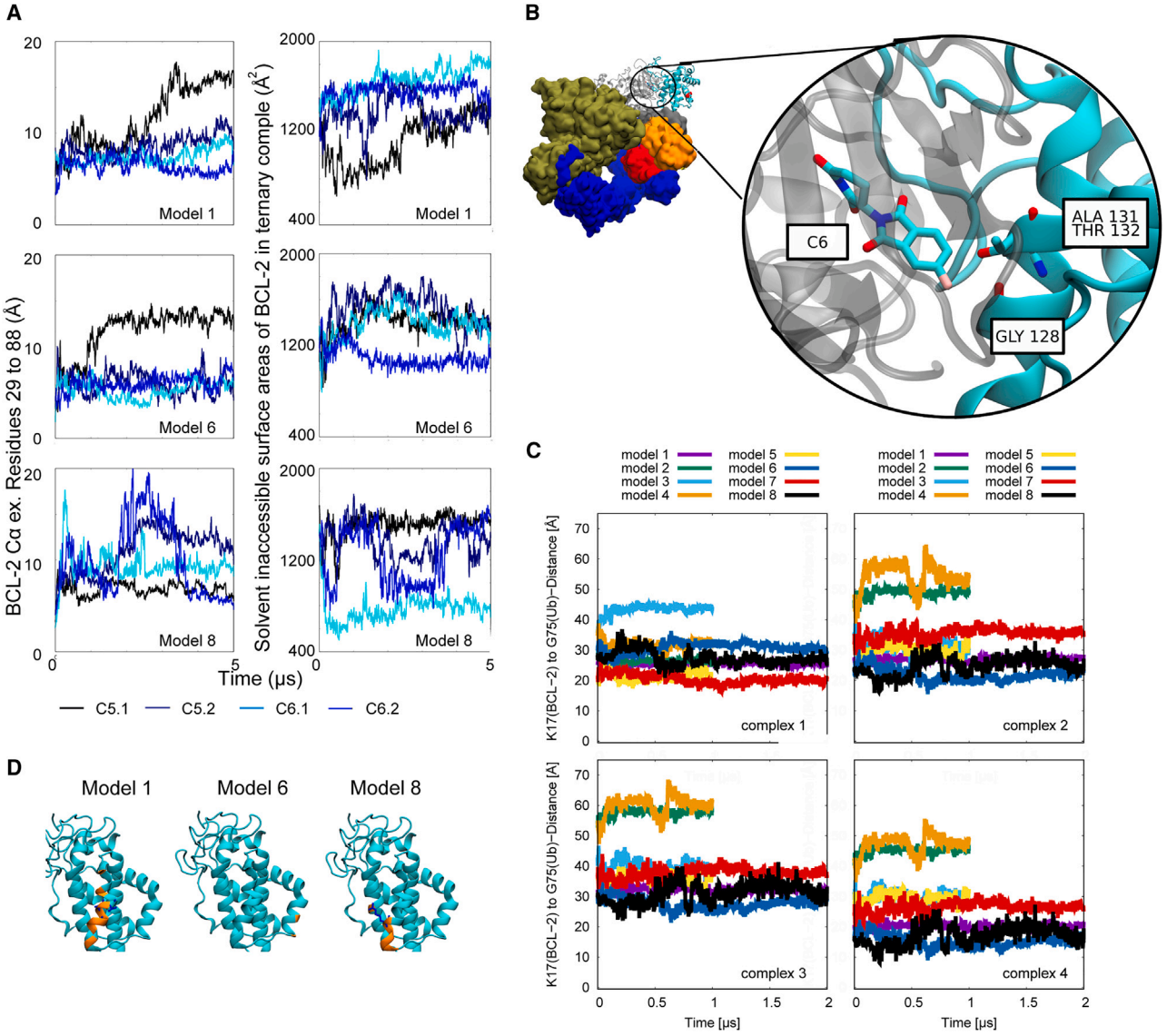

Figure 4. Molecular modeling study

(A) Cα RMSD and solvent-inaccessible surface area of BCL-2 for different ternary complex models during the MD simulations. Cα RMSD was calculated for BCL-2 without the unstructured loop region from residues 29 to 88. Simulations were aligned onto CRBN from the initial complex structures determined from docking with ClusPro. Cα RMSD values were calculated to the BCL-2 position in the corresponding initial complex model. C5 and C6 represent the ligand, 1 or 2 the different fluorine positions in the initial ternary complex model. Models 1, 6, and 8 were simulated with all possible fluorine positions. The solvent-inaccessible surface area was determined as the difference in the solvent-accessible areas of BCL-2 isolated and in the ternary complex for each individual frame (isolated - complex). RMSDs are in Å, solvent-inaccessible area in $Å^2$, and time in μs. Data were processed with a moving average over 10 ns (10 frames).

(B) Model for E3 ligase complex with BCL-2 and molecular glue. BCL-2 (cyan), molecular glue C6 (violet), CRBN (light gray), DDB1 (tan), Cullin-1 (blue), UBE2D2 (orange), NEDD8 (red), RBX1 (dark gray), and "Ub" (yellow). BCL-2 Cα atoms of K17 and K22 are shown as red spheres. Dashed lines indicate the distance to Ub.

(C) Cα distance of K17 from BCL-2 to G75 from ubiquitin in the four different E3-ligase complexes for the eight different BCL-2:C6:CRBN complex models. Cα distances between K17 of the BCL-2 protein to the G75 of ubiquitin in the modeled complexes. Simulations of the ternary BCL-2:C6:CRBN complex were aligned onto the static CRBN of the E3-ligase complex. Simulations were performed for 1 μs and extended for selected models to 2 μs (models 1, 6, 7, and 8). Distances are in Å and time in μs.

(D) BCL-2 interacting residues with C5 and C6 ligands during the simulations for three different ternary complex models (models 1, 6, and 8). BCL-2 Cα atoms that were within 6 Å of the ligand for at least 3 μs simulation time are shown in orange. Residues within the same time and within 4 Å of the fluorine of C5 and/or C6 are shown in blue. Note that model 6 has no residues within 4 Å of the C5/6 fluorine. See also Figure S5.

its orientation during the initial MD stimulations of the BCL-2:C6:CRBN complexes. To test for different fluoro-phthalimide orientations in the binding site, the C5 and C6 phthalimide moieties were vertically flipped around the phthalimide plane in the initial starting structures for models 1, 6, and 8 and simulated for 5.0 μs (Figure S5C). Here, the phthalimide rings of C5 and C6 also maintained their initial orientations. The BCL-2 protein moved significantly from the initial position for model 8 while for models 1 and 6 only the ternary complex containing 3-fluoro-phthalimide (Figure 4A, C5.1) explores larger rearrangements, as manifested in the BCL-2 Cα position RMSD values to the initial docked protein:protein structures. Nonetheless, all complexes maintain protein:protein contacts and reveal BCL-2:CRBN solvent-inaccessible interfaces through the entire 5.0 μs simulation times (Figure 4A).

Extended MD simulations of selected ternary complex models indicate potential interacting BCL-2 residues between PRO123 to ARG139 with the molecular glues. For every frame of the simulated model complexes, each BCL-2 Cα atom within 6 Å to the ligand was determined. Potentially interacting residues were classified if the residue was at least 8 μs of cumulated C5 or C6 simulation times in 6 Å proximity to the ligand, revealing for model 1: ARG139, GLU136, GLU135, THR132, ALA131, PHE130, ARG129, GLY128, ARG127, THR125; model 6: GLU114, GLN118; model 8: TRP176, GLY128, ARG127, ALA126, THR125, PHE124 (Figure 4D). In addition, every residue within 4 Å distance to the fluorine of C5 or C6 was determined. We found that ARG127 (model 8), GLY128 (model 1), ALA131 (model 1), and THR132 (model 1) satisfied the aforementioned criteria (Figure 4D), indicating potential interactions with the fluorine of C5 and C6.

Interactions of the glue with GLY128 (BCL-2) are of special interest, as the previously reported degron for thalidomide-based molecular glues is a β-hairpin with the CxxCG sequence, where the glue packs against the glycine.[29] BCL-2 does not contain a CxxCG sequence, nor a β-hairpin structural motive. So, the observed proximity of the C5 and C6 molecular glue to GLY128 potentially hints at a new degron motive, where the packing of C5 and C6 against a helical glycine in the TXXGXXXT sequence shows a similarity with the motifs known from the literature.[15]

To elucidate the contribution of different BH domains in C5-mediated degradation, we engineered four BCL-2 variants with EGFP tags, each lacking one of the BH domains (Figure 5A). Our finding showed that C5 significantly diminished the EGFP intensity in cells expressing either BCL-2$^{\Delta BH2}$ or BCL-2$^{\Delta BH3}$. However, cells expressing variants missing BH1 (BCL-2$^{\Delta BH1}$) and or BH4 (BCL-2$^{\Delta BH4}$) were unaffected by C5 treatment (Figures 5B, 5C, and S5D). Moreover, Our FRET assay results clearly showed that the disruption of the CRBN-BCL-2 interaction occurred exclusively in cells expressing BCL-2$^{\Delta BH1}$ (Figure 5D), which was confirmed by co-immunoprecipitation of CRBN and BCL-2-EGFP (Figure 5E), suggesting a predominant role of the BH1 domain majorly in facilitating the C5-mediated CRBN-BCL-2 interaction. The resistance of the BCL-2$^{\Delta BH4}$ to C5 is likely due to the absence of K17 and K22 (Figure 5B).

Our molecular modeling data suggested the potential involvement of G128, A131, and T132 in C5-induced BCL-2 degradation (Figure 4B). To test this hypothesis, we generated mutations G128L, A131L, T132L, and a triple mutation of GAT-LLL. The results from the EGFP depletion assay and FRET assay consistently showed only a slight reduction in fluorescence signal intensity in cells expressing the single mutations. In contrast a significant reduction was found in cells with the triple mutations (Figures 5F and 5G). This was further confirmed by co-immunoprecipitation of CRBN

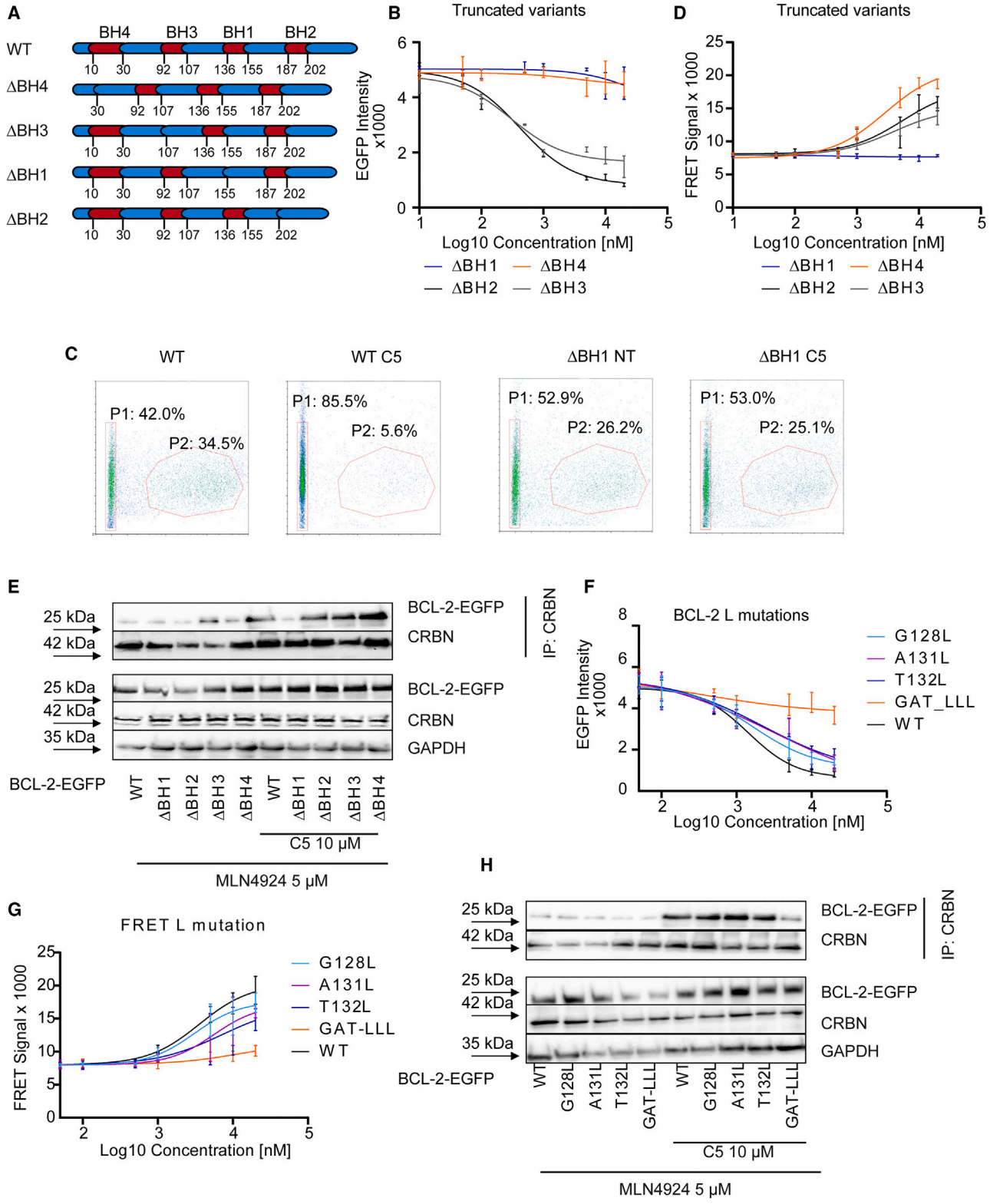

Figure 5. GLY128, ALA131, and THR132 are crucial for BCL-2 degradation

(A) Illustration of truncated BCL2 variants, ΔBH1, ΔBH2, ΔBH3, and ΔBH4 with the indicators (in red) of the numbers of amino acids.

(B) Fluorescence intensity of BCL-2$^{\Delta BH1}$-, BCL-2$^{\Delta BH2}$-, BCL-2$^{\Delta BH3}$-, or BCL-2$^{\Delta BH4}$-EGFP in the presence of C5 (n = 3).

Figure 5. *Continued*

(C) Percentage of cells expressing BCL-2^{WT} or BCL-$2^{\Delta BH1}$-EGFP treated with C5 (10 μM, overnight) in Kelly cells. DMSO was used as control (n = 2). P1, gate of GFP– cells; P2, gate of GFP+ cells.

(D) FRET intensity of cells expressing BCL-$2^{\Delta BH1}$-, BCL-$2^{\Delta BH2}$-, BCL-$2^{\Delta BH3}$-, or BCL-$2^{\Delta BH4}$-EGFP in the presence of C5 and MLN4924 (n = 3).

(E) C5-mediated interaction between CRBN and BCL-2 variants. HEK293 cells were transfected with BCL-2^{WT}-, BCL-$2^{\Delta BH1}$-, BCL-$2^{\Delta BH2}$-, BCL-$2^{\Delta BH3}$-, or BCL-$2^{\Delta BH4}$-EGFP and treated with C5 in the presence of MLN4924 (5 μM). CRBN antibody was used for immunoprecipitation.

(F) EGFP intensity of BCL-2^{WT}-, BCL-2^{G128L}-, BCL-2^{A131L}-, BCL-2^{T132L}-, or BCL-$2^{GAT-LLL}$-EGFP in the presence of C5 (n = 3).

(G) FRET intensity of cells expressing BCL-2^{WT}-, BCL-2^{G128L}-, BCL-2^{A131L}-, BCL-2^{T132L}-, or BCL-$2^{GAT-LLL}$-EGFP in the presence of C5 and MLN4924 (n = 3).

(H) C5-mediated interaction between CRBN and BCL-2 variants. HEK293 cells were transfected with BCL-2^{WT}-, BCL-2^{G128L}-, BCL-2^{A131L}-, BCL-2^{T132L}-, or BCL-$2^{GAT-LLL}$-EGFP and treated with C5 in the presence of MLN4924 (5 μM). CRBN antibody was used for immunoprecipitation. Data are represented as mean ± SEM. See also Figure S5.

and BCL-2-EGFP (Figure 5H), underscoring the critical roles of these three amino acids in the C5-mediated BCL-2 degradation.

Anti-tumor activity of C5 in cells and *Drosophila*

BCL-2 stands out as a prominent anti-apoptotic protein in various cancer types.[1] Venetoclax, functioning as a BH3 mimic, effectively inhibits the activity of BCL-2^{WT} in Kelly cells. This inhibition led to cell death with comparable IC_{50} values, approximately 4 μM, in both $CRBN^{WT}$ and $CRBN^{KO}$ cells, as depicted in Figure 6A, in accordance with previous reports.[30]

Overexpression of BCL-2 (BCL-2^{OE}) induced roughly a 5-fold resistance to venetoclax, as illustrated in Figure 6B. Furthermore, resistance is further increased in cells expressing BCL-2^{G101V}, as demonstrated in Figure 6C, in line with findings indicating diminished inhibition by venetoclax for the BCL-2^{G101V} variant.[7] Notably, the presence of CRBN appeared to have no significant impact on venetoclax-induced cell death (Figures 6A–6C). In contrast, C5-induced cell death exhibited a strong correlation with CRBN expression, evident in the distinct resistance observed in corresponding Kelly $CRBN^{WT}$ and $CRBN^{KO}$ cells (Figures 6A–6C). Upon evaluating Kelly $CRBN^{WT}$ cells, overexpressing BCL-2 (BCL-2^{OE}) or containing the BCL-2^{G101V} mutation, a mild reduction of approximately 1.5-fold in C5 toxicity is observed (Figures 6B and 6C). This observation was consistent with our finding that comparable C5-mediated BCL-2 degradation occurred in both Kelly BCL-2^{OE} and BCL-2^{G101V} cells. Caspase-3/7 cleavage serves as a hallmark of apoptosis.[31] Analyzing this apoptosis marker further validated that C5-mediated apoptosis was equally prevalent in both BCL-2^{OE} and BCL-2^{G101V} cells. However, this phenomenon was heavily reliant on the presence of CRBN, as depicted in Figure 6D.

Recent research has harnessed the sophisticated genetic system of *Drosophila* to model human diseases with the aim of exploring the pathogenic mechanism and assessing drug efficacy.[12,32–35] Notably, mutations in the Notch pathway give rise to intestinal tumors in *Drosophila* characterized by an accumulation of undifferentiated stem cell progenies.[12,36] During the initial stage of tumor growth, autocrine activation of the EGF pathway was observed.[34,36] Given that EGF can recruit members of the BCL-2 family for cell growth and anti-apoptosis, and considering the conserved CRBN signaling pathway between *Drosophila* and humans, as demonstrated in our previous study,[12,37,38] we examined the anti-tumor effect of C5 in our previously established *Drosophila* intestinal tumor model induced by the depletion of Notch.[12,36] To initiate our investigation, we assessed the *in vivo* cellular toxicity of C5 by administering it orally to wild-type flies. Venetoclax and thalidomide were used as reference compounds. We found that the ingestion of venetoclax and thalidomide led to reduced stem cell activity, as demonstrated by a decrease in the number of phosphor-histone 3-positive cells in the intestine (Figures S6A and S6B). In contrast, the

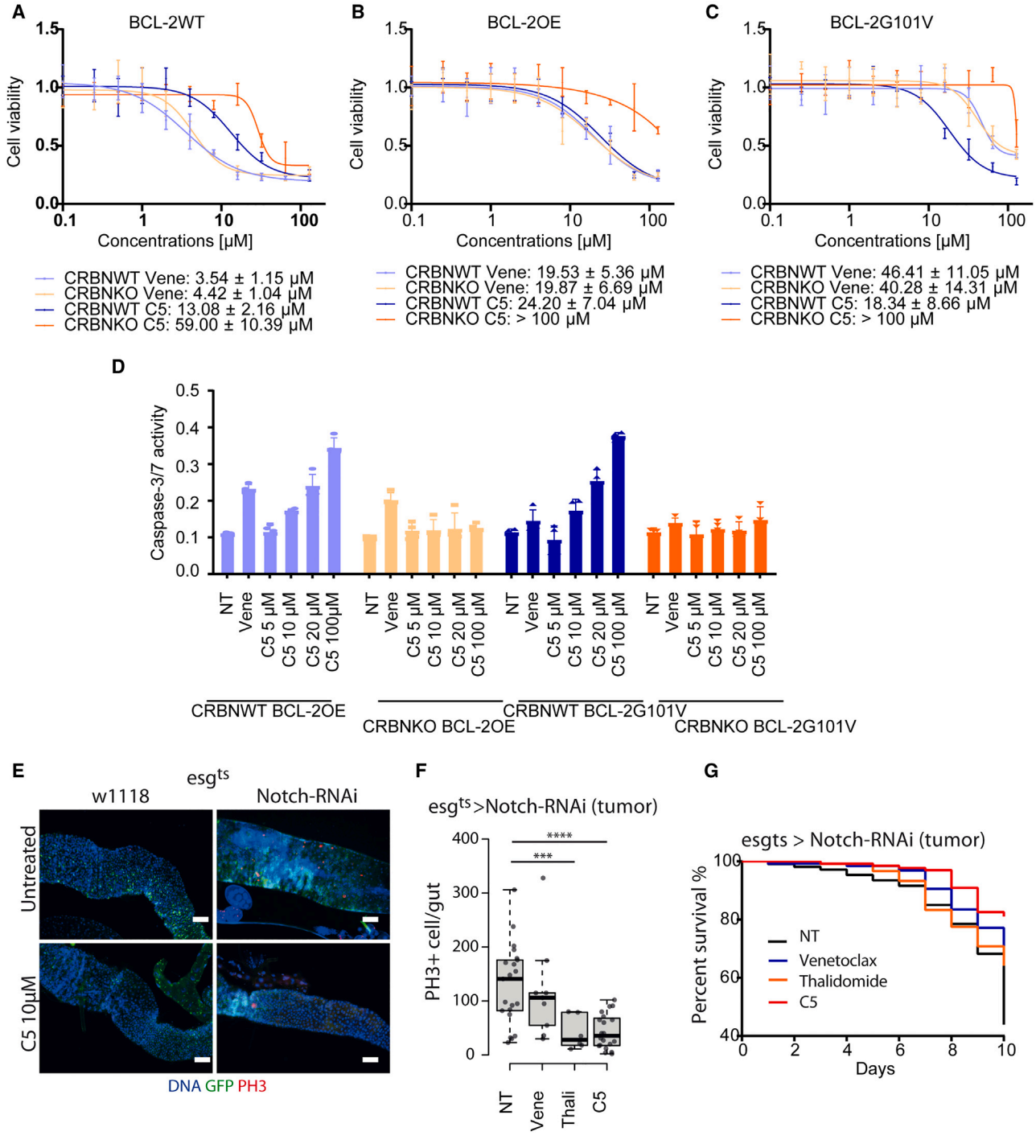

Figure 6. Anti-tumor activity of C5 in cells and *Drosophila*

(A) Comparison of cytotoxicity of venetoclax (Vene) and C5 (48 h) in Kelly cells expressing $CRBN^{WT}$ or $CRBN^{KO}$.

(B) Comparison of cytotoxicity of Vene and C5 in Kelly BCL-2^{OE} cells expressing $CRBN^{WT}$ or $CRBN^{KO}$.

(C) Comparison of cytotoxicity of Vene and C5 in Kelly BCL-2^{G101V} cells expressing $CRBN^{WT}$ or $CRBN^{KO}$.

(D) Evaluation of caspase-3/7 activity in Kelly BCL-2^{OE}/$CRBN^{WT}$, BCL-2^{OE}/$CRBN^{KO}$, BCL-2^{G101V}/$CRBN^{WT}$, or BCL-2^{G101V}/$CRBN^{KO}$ cells. Cells treated with increasing concentrations of C5. Vene (20 μM) was used as control.

(E) The representative image of the posterior midgut of control (*esg^{ts}>w1118*) and tumor flies (*esg^{ts}>Notch-RNAi*) in the mock and BCL-2 inhibitor C5 (10 μM) treatment conditions at 29°C for 7 days, and stained with phosphor-histone 3 (PH3) in red, stem cells are marked by GFP in green, nuclei are stained with DAPI in blue. Scale bars, 40 μm.

Figure 6. *Continued*

(F) Quantification of PH3-positive cells of whole midgut of tumor flies with the indicated treatments at 29°C for 7 days. Significant differences between treatment and the control group are indicated with asterisks (***$p < 0.001$, ****$p < 0.0001$).

(G) The BCL-2 inhibitor C5 treatment rescues Notch-defective tumor-induced early mortality. Number of flies used in the experiment: non-treated group, $n = 107$; venetoclax group, $n = 127$; thalidomide group, $n = 120$; C5 group, $n = 132$. The flies were flipped to freshly prepared solution every day and the survival rate was monitored every day. Data are represented as mean ± SEM. See also Figure S6.

administration of C5 had minimal effects on stem cell activity under the same conditions (Figure S6A). In the context of Notch-depleted intestinal tumorigenesis, the ingestion of C5 resulted in a significant reduction in intestinal tumor growth, accompanied by decreased stem cell activity and a lower mortality rate among tumor-bearing flies (Figures 6E–6G). These findings suggest that C5 may specifically target the proliferative stem cells or undifferentiated stem cell progenies.

DISCUSSION

The BCL-2 family of proteins plays a pivotal role in regulating cell death, encompassing various mechanisms such as apoptosis, necrosis, and autophagy.[1] BCL-2 is a key member of the pro-survival protein class of the BCL-2 family.[3] Mechanistically, BCL-2 protein prevents cell death by binding to BH3 motifs in specific BH3-binding grooves, thereby inhibiting pro-apoptotic proteins, such as BAX and BAK.[3] Initially, BH3 mimetics, such as ABT-737 and ABT-263, targeting multiple pro-survival proteins, were developed.[39] However, their clinical application was limited due to thrombocytopenia resulting from BCL-XL inhibition.[40] This limitation led to the development of venetoclax, which selectively targets BCL-2, sparing platelets while inducing apoptosis in cancer cells,[3] demonstrating rapid clinical responses with ~20% complete remission as monotherapy or up to 50% when combined with rituximab.[41,42] However, acquired mutations, such as F104C observed in a mouse model[43] and G101V in patients with leukemia recurrence[44] necessitate the development of new strategies for treating BCL-2-related cancers.

Recently, chemical protein degraders, including MGDs and PROTACs, have merged as novel small-molecule-based approaches to degrade both wild-type and mutated proteins,[12] including a few BCL-2 PROTACs reported recently.[19–21] In this study, we conducted a comprehensive proteome-wide screening and discovered that specific thalidomide analogs (C5, C6, and C7) demonstrated effective degradation of BCL-2 in cancer cells without affecting other BCL-2 family members such as BCL-XL, BAD, or BAX. It has been observed that lenalidomide can induce the degradation of the kinase CK1, while its analogs thalidomide and pomalidomide do not have the same effect.[16] Similarly, we found that C5 induced complex formation of BCL-2 and CRBN *in vitro* and in cells, while thalidomide and its methylation-inactivated derivative did not facilitate this interaction. This underscores how even slight variances in chemical structure can lead to significant distinctions in the specific proteins targeted for degradation.[22]

Event-driven mechanism is one of the major advantages of chemical protein degraders, enabling to target mutated proteins even with low binding affinity.[12,45,46] We demonstrated that C5 affected the stability of venetoclax-resistant BCL-2 variants, G101V and F104C, similarly to BCL-2^{WT}, via the CRBN-dependent ubiquitin-proteasome pathway. As a result, cells expressing BCL-2^{G101V} were susceptible to C5, while refractory to venetoclax or BCL2-PROTAC based on BH3 mimics. K17 plays an important role in BCL-2 ubiquitination.[20,26] In agreement, BCL-$2^{\Delta BH4}$ and BCL-2^{K17R} showed resistance to C5. Moreover, mutation at K22 also conferred resistance to degradation, suggesting that both K17 and K22, as well as the BH4 domain

where both mutations are located, are indispensable for C5-mediated BCL-2 ubiquitination. Krönke et al. have elucidated that the CxxCG sequence shared within C2H2-type ZF transcription factors serves as the degron responsible for interaction with thalidomide and its derivatives.[10] It is tempting to speculate on a novel degron motive, as our molecular modeling indicates the glue binding to a helical glycine flanked by threonines, which was further confirmed by triple mutation of GLY128L, ALA131L, and THR132L, suggesting the potential to interact of C5/C6 with BCL-2^{G128} in close proximity to the BH1 domain, analogous to established motifs.[15]

Patel et al. and Zhou et al. demonstrated that EGF and JNK play significant roles in promoting tumorigenesis in *Drosophila* intestinal tumor models induced by Notch mutations[36] or depletion.[34] Interestingly, administration of C5 resulted in reduction of cancer stem cells, accompanied by an increase in the survival rate in this *Drosophila* intestinal tumor model, in agreement with previous findings that EGF and/or JNK recruited members of the BCL-2 family, including BCL-2, to sustain tumor cell proliferation.[38,47]

In conclusion, our study convincingly demonstrates that thalidomide analogs, such as C5, have the potential to effectively degrade BCL-2 and its resistant mutants in a CRBN-dependent manner, offering a promising approach for cancer therapy. The study provides valuable insights into the mechanisms of action of these compounds, highlighting the importance of the BH1 domain in BCL-2 degradation and the involvement of specific lysine residues. These findings contribute to the development of targeted therapies for cancer patients, especially those resistant to existing treatments.

EXPERIMENTAL PROCEDURES

Resource availability

Lead contact

Further information and requests for resources and reagents should be directed to and will be fulfilled by the lead contact, Xinlai Cheng (Cheng@pharmchem.uni-frankfurt.de).

Materials availability

All unique/stable reagents generated in this study are available from the lead contact with a completed materials transfer agreement.

Data and code availability

The proteomics data have been deposited at PRIDE under PXD051025 and are publicly available as of the date of publication. This paper does not report original code.

Materials

Kelly $CRBN^{WT}$ and $CRBN^{KO}$ cells were gifts from the Eric Fisher lab (Department of Medical Oncology, Dana-Farber Cancer Institute, Boston, MA). BCL-2^{WT}-EGFP was purchased from Addgene (no. 17999). BCL-2^{G101V}, BCL-2^{F104C}, BCL-2^{K17R}, BCL-2^{K22R}, BCL-$2^{\Delta BH1}$, BCL-$2^{\Delta BH2}$, BCL-$2^{\Delta BH3}$, and BCL-$2^{\Delta BH4}$ plasmids were made and validated by Genscript (Dutch). CRBN-FLAG (no. 100329) and BRD4-GST (no. 31044) were purchased from BPS Bioscience. BCL-2GST (no. SRP5340) was purchased from Sigma-Aldrich (Germany). Thaliomide (no. HY-14658), lenalidomide (no. HY-A0003), pomalidomide (no. HY-10984), C5 (no. HY-41547), C6 (no. HY-W087383), C7 (no. HY-126457), and venetoclax (no. HY-15531) were purchased MedChemExpress (Sweden). BCL-2 (no. 15071), BCL-XL (no. 2764), BAD (no. 9239), BAX (no. 5023), and IKZF3 (no. 15103) were purchased from Cell

Technologies. Ubiquitin was purchased from Abcam (ab137031). ZNF490 (SAB1407789-50UG) was purchased from Sigma-Aldrich (Germany). Actin (no. SC-4778) and vinculin (no. 73614) were purchased from Santa Cruz Biotechnology (Germany). CRBN-OFP was reported previously.[12]

Cell culture and transfection

HEK293T cells were cultured in DMEM supplemented with 10% FBS and 100 mg/U/mL (1%) penicillin/streptomycin (Pen/Strep). THP-1 cells, Jurkat cells, and Kelly cells were cultivated in RPMI 1640. All cultures were maintained in a controlled environment of 5% CO_2 at 37°C with high humidity.

The transfection process for plasmid overexpression followed a previously established protocol.[48] Initially, cells were seeded in 6-well plates at a density of 300,000 cells per well and incubated overnight. Lipofectamine 3000 served as the transfection reagent (Thermo Fisher Scientific, L300015). Lipofectamine (6 μL) was added to tube I with 50 μL of Opti-MEM medium. In tube II, 6 μL of P3000 and 5,000 ng of plasmid were combined with 50 μL of Opti-MEM medium. The contents of tube II were subsequently added to tube I, and the mixture was incubated at room temperature for 5–10 min. Following transfection, the cell culture medium was refreshed with 1.5 mL of DMEM containing 10% FCS without Pen/Strep. The transfection mixture was added to the cells and incubated overnight. Subsequently, the medium was replaced with DMEM containing 10% FCS and 1% Pen/Strep, and cells were further incubated for an additional 24–48 h.

NanoBRET assay

The assay was performed as described previously.[49] In brief, full-length CRBN was obtained as plasmids cloned in frame with a terminal NanoLuc-fusion (Promega, no. N2741). The plasmid was transfected along with full-length DDB1 into HEK293T cells using FuGENE HD (Promega, no. E2312) and proteins were allowed to express for 20 h. Serially diluted inhibitor and NanoBRET CRBN Tracer (Promega) at a concentration determined previously as the Tracer IC_{50} (500 nM) were pipetted into white 384-well plates (Greiner no. 781207) using an Echo acoustic dispenser (Labcyte). The corresponding protein-transfected cells were added and reseeded at a density of 2×10^5 cells/mL after trypsinization and resuspending in Opti-MEM without phenol red (Life Technologies). The system was allowed to equilibrate for 2 h at 37°C/5% CO_2 prior to BRET measurements. To measure BRET, NanoBRET NanoGlo Substrate + Extracellular NanoLuc Inhibitor (Promega, no. N2540) was added as per the manufacturer's protocol, and filtered luminescence was measured on a PHERAstar plate reader (BMG Labtech) equipped with a luminescence filter pair (450 nm BP filter [donor] and 610 nm LP filter [acceptor]). Competitive displacement data were then graphed using GraphPad Prism 9 software using a normalized three-parameter curve fit with the following equation: $y = 100/(1 + 10^{(x-LogIC50)})$.

Alpha assay

The CRBN-FLAG and BCL-2GST proteins were both diluted to a concentration of 100 nM in an alphaLISA PPI buffer (no. AL015C), which consisted of 250 mM HEPES (pH 7.3), 500 mM NaCl, 2.5% Triton X-100, and 2.5% BSA. A mixture comprising 10 nM of CRBN-FLAG and 10 nM BCL-2GST in 9 μL of the PPI buffer was then exposed to increasing concentrations of either thalidomide or C5 (1 μL of either compound). Subsequently, this reaction mixture was incubated at room temperature for a duration of 60 min. Following this initial incubation period, 1 μL of GST-acceptor beads (at a concentration of 500 μg/mL) (PerkinElmer, no. AL110C) and 1 μL of FLAG-donor beads (at a concentration of 500 μg/mL)

(PerkinElmer, no. AS103D) were introduced into the reaction buffer. This new mixture was once again incubated at room temperature for another 60 min. Finally, the plate reader utilized for this experiment was the Alphaplate-384 (PerkinElmer, no. 6005350), with an excitation/emission wavelength of 680 nm/615 nm.

Immunoprecipitation

HEK293T cells were initially seeded in a 6-well plate at a density of 300,000 cells per well and incubated overnight. Subsequently, they were transfected with a mixture of Lipofectamine 3000 and reagent (6 μL of each) and a BCL-2 DNA plasmid (2,500 ng) in RPMI 1640 containing 10% FBS (without Pen/Strep). After 24 h, the medium was refreshed with medium containing 10% FBS and 1% Pen/Strep. The cells were further incubated for an additional 24 h and treated with thalidomide (10 μM) or varying concentrations of C5 in the presence or absence of MG132. The cells were then lysed in an immunoprecipitation lysis buffer (comprising 20 mM Tris-HCl [pH 8], 150 mM NaCl, 1% Nonidet P-40, and 2 mM EDTA). A cocktail of protease and protein-phosphatase inhibitors was freshly added, including 5 mM NaF, 1 mM Na_3VO_4, 10 mg/mL pepstatin, 100 mM PMSF, and 3 mg/mL aprotinin.

A pre-cleaning step was performed by adding 20 μL rabbit serum for 1 h at 4°C and then incubated with 20 μL of protein A magnetic beads for 30 min at 4°C. The supernatant was incubated with 2 μL BCL-2 antibody with gentle rocking overnight at 4°C. Protein A magnetic beads were added and incubated for 1–3 h at 4°C. The pellet was washed several times with lysis buffer and re-suspended in the loading buffer and heated to 95°C for 3 min.

Immunoblotting

As described previously,[48] cell lysis was executed using a urea-lysis buffer containing the following components: 1 mM EDTA, 0.5% Triton X-100, 5 mM NaF, 6 M urea, 1 mM Na_3VO_4, 10 mg/mL pepstatin, 100 mM PMSF, and 3 mg/mL aprotinin in PBS. Blot detection was carried out using enhanced chemiluminescence. A total of 40 mg of total protein was separated on either 8%, 10%, or 12% SDS-PAGE gels, followed by subsequent immunoblotting with specific antibodies. β-Actin, GAPDH, or vinculin antibody served as the loading control. Primary antibodies (diluted 1:1,000) were incubated overnight at 4°C in TBS (pH 7.5) with 0.1% Tween 20 and 5% BSA/milk. Secondary antibodies (diluted 1:10,000, Dianova, Germany) were incubated in TBS (pH 7.5) with 5% milk and 0.1% Tween 20 for 1 h at room temperature.

Immunofluorescence for GFP detection

The Kelly cells were transfected with various BCL-2 GFP plasmids and were then cultured in full culture medium for 48 h. Afterward, these cells were subjected to the compound treatment as detailed in the main text.

For plate reader or fluorescence microscope analysis, we utilized a 96-well black plate. Initially, the cells were fixed with 4% paraformaldehyde for 10 min and then rinsed with a solution of 1% BSA in PBS. To stain the DNA, Hoechst 33342 (1 μg/mL, Sigma Aldrich, no. 1234011) was utilized. Signals or images were captured either using a plate reader equipped with a GFP filter (Ex/Em, 488 nm/510 nm) or a fluorescence microscope.

For fluorescence-activated cell sorting analysis, the cells were trypsinized, resuspended, and fixed in PBS containing 1% BSA.

FRET assay

The FRET assay was performed as reported previously.[12] HEK293, Kelly, or K562 cells were seeded in a black 96-well plate at a density of 15,000 cells/well. The cells were transfected with $CRBN^{OFP}$ and various $BCL\text{-}2^{GFP}$ constructs, as described above. After 48 h, the cells were treated with increasing concentrations of C5 or thalidomide for 16 h combined with MLN4924 to block the degradation. FRET signals were recorded by a plate reader (Ex/Em, 488 nm/573 nm).

SUPPLEMENTAL INFORMATION

Supplemental information can be found online at https://doi.org/10.1016/j.xcrp.2024.101960.

ACKNOWLEDGMENTS

We thank Dr. Stefan Knapp for his great help and Daniel Schaefer for preparing the screening. We thank the Bloomington Drosophila Stock Center, Vienna Drosophila RNAi Center (VDRC), and Bruce Edgar (Utah University, USA) for fly stocks. We thank Yansong Xiong and the Analytical Instrumentation Center of Hunan University for assistance in confocal microscopy. This work was supported by DFG grant program (CH 1690/2-3 and 4-1) to X.C.; BMBF-ProxiDrugs (03ZU1109EA) to I.D., G.H., and X.C.; and LOEWE Center Frankfurt Cancer Institute (FCI) funded by the Hessen State Ministry of Higher Education, Research and the Arts (III L 5–519/03/03.001 - (0015)) to X.C. M.H., and G.H. were also supported by the Max Planck Society. The work from Zhou Laboratory is supported by Startup funding from Hunan University, National Natural Science Foundation of China (32270890), and the Department of Science and Technology of Hunan Province (2023JJ0007).

AUTHOR CONTRIBUTIONS

Conceptualization, X.C.; methodology – biochemistry and cellular experiments, J.W. and X.C.; methodology – molecular modeling, M.H. and G.H.; methodology – *Drosophila* experiments, K.H. and J.Z.; methodology – proteomics, V.J.S., R.R., and I.D.; methodology – chemical synthesis, S.H.; methodology – nanobret assay, M.P.S.; writing – original draft, M.H., J.Z., and X.C.; writing – review & editing, X.C.; funding acquisition, G.H., J.Z., I.D., and X.C.; supervision, X.C.

DECLARATION OF INTERESTS

The authors declare no competing interests.

Received: October 31, 2023
Revised: February 10, 2024
Accepted: April 13, 2024
Published: May 2, 2024

REFERENCES

1. Juin, P., Geneste, O., Gautier, F., Depil, S., and Campone, M. (2013). Decoding and unlocking the BCL-2 dependency of cancer cells. Nat. Rev. Cancer *13*, 455–465. https://doi.org/10.1038/nrc3538.

2. Karjalainen, R., Liu, M., Kumar, A., He, L., Malani, D., Parsons, A., Kontro, M., Kallioniemi, O., Porkka, K., and Heckman, C.A. (2019). Elevated expression of S100A8 and S100A9 correlates with resistance to the BCL-2 inhibitor venetoclax in AML. Leukemia *33*, 2548–2553. https://doi.org/10.1038/s41375-019-0504-y.

3. Vogler, M., Dinsdale, D., Dyer, M.J.S., and Cohen, G.M. (2009). Bcl-2 inhibitors: small molecules with a big impact on cancer therapy. Cell Death Differ. *16*, 360–367. https://doi.org/10.1038/cdd.2008.137.

4. Mullard, A. (2016). Pioneering apoptosis-targeted cancer drug poised for FDA approval. Nat. Rev. Drug Discov. *15*, 147–149. https://doi.org/10.1038/nrd.2016.23.

5. Souers, A.J., Leverson, J.D., Boghaert, E.R., Ackler, S.L., Catron, N.D., Chen, J., Dayton, B.D., Ding, H., Enschede, S.H., Fairbrother, W.J., et al. (2013). ABT-199, a potent and selective BCL-2 inhibitor, achieves antitumor activity while sparing platelets. Nat. Med. *19*, 202–208. https://doi.org/10.1038/nm.3048.

6. Lessene, G., Czabotar, P.E., Sleebs, B.E., Zobel, K., Lowes, K.N., Adams, J.M., Baell, J.B., Colman, P.M., Deshayes, K., Fairbrother, W.J., et al. (2013). Structure-guided design of a selective BCL-X(L) inhibitor. Nat. Chem. Biol. *9*, 390–397. https://doi.org/10.1038/nchembio.1246.

7. Birkinshaw, R.W., Gong, J.N., Luo, C.S., Lio, D., White, C.A., Anderson, M.A., Blombery, P., Lessene, G., Majewski, I.J., Thijssen, R., et al. (2019). Structures of BCL-2 in complex with venetoclax reveal the molecular basis of resistance mutations. Nat. Commun. *10*, 2385. https://doi.org/10.1038/s41467-019-10363-1.

8. Tausch, E., Close, W., Dolnik, A., Bloehdorn, J., Chyla, B., Bullinger, L., Döhner, H., Mertens, D., and Stilgenbauer, S. (2019). Venetoclax resistance and acquired BCL2 mutations in chronic lymphocytic leukemia. Haematologica *104*, e434–e437. https://doi.org/10.3324/haematol.2019.222588.

9. Fischer, E.S., Böhm, K., Lydeard, J.R., Yang, H., Stadler, M.B., Cavadini, S., Nagel, J., Serluca, F., Acker, V., Lingaraju, G.M., et al. (2014). Structure of the DDB1-CRBN E3 ubiquitin ligase in complex with thalidomide. Nature *512*, 49–53. https://doi.org/10.1038/nature13527.

10. Krönke, J., Udeshi, N.D., Narla, A., Grauman, P., Hurst, S.N., McConkey, M., Svinkina, T., Heckl, D., Comer, E., Li, X., et al. (2014). Lenalidomide causes selective degradation of IKZF1 and IKZF3 in multiple myeloma cells. Science *343*, 301–305. https://doi.org/10.1126/science.1244851.

11. Lu, G., Middleton, R.E., Sun, H., Naniong, M., Ott, C.J., Mitsiades, C.S., Wong, K.K., Bradner, J.E., and Kaelin, W.G., Jr. (2014). The myeloma drug lenalidomide promotes the cereblon-dependent destruction of Ikaros proteins. Science *343*, 305–309. https://doi.org/10.1126/science.1244917.

12. Gama-Brambila, R.A., Chen, J., Zhou, J., Tascher, G., Münch, C., and Cheng, X. (2021). A PROTAC targets splicing factor 3B1. Cell Chem. Biol. *28*, 1616–1627.e8. https://doi.org/10.1016/j.chembiol.2021.04.018.

13. Gama-Brambila, R.A., Chen, J., Dabiri, Y., Tascher, G., Němec, V., Münch, C., Song, G., Knapp, S., and Cheng, X. (2021). A Chemical Toolbox for Labeling and Degrading Engineered Cas Proteins. JACS Au *1*, 777–785. https://doi.org/10.1021/jacsau.1c00007.

14. Winter, G.E., Buckley, D.L., Paulk, J., Roberts, J.M., Souza, A., Dhe-Paganon, S., and Bradner, J.E. (2015). DRUG DEVELOPMENT. Phthalimide conjugation as a strategy for in vivo target protein degradation. Science *348*, 1376–1381. https://doi.org/10.1126/science.aab1433.

15. Sievers, Q.L., Petzold, G., Bunker, R.D., Renneville, A., Słabicki, M., Liddicoat, B.J., Abdulrahman, W., Mikkelsen, T., Ebert, B.L., and Thomä, N.H. (2018). Defining the human C2H2 zinc finger degrome targeted by thalidomide analogs through CRBN. Science *362*, eaat0572. https://doi.org/10.1126/science.aat0572.

16. Krönke, J., Fink, E.C., Hollenbach, P.W., MacBeth, K.J., Hurst, S.N., Udeshi, N.D., Chamberlain, P.P., Mani, D.R., Man, H.W., Gandhi, A.K., et al. (2015). Lenalidomide induces ubiquitination and degradation of CK1alpha in del(5q) MDS. Nature *523*, 183–188. https://doi.org/10.1038/nature14610.

17. Matyskiela, M.E., Couto, S., Zheng, X., Lu, G., Hui, J., Stamp, K., Drew, C., Ren, Y., Wang, M., Carpenter, A., et al. (2018). SALL4 mediates teratogenicity as a thalidomide-dependent cereblon substrate. Nat. Chem. Biol. *14*, 981–987. https://doi.org/10.1038/s41589-018-0129-x.

18. Donovan, K.A., An, J., Nowak, R.P., Yuan, J.C., Fink, E.C., Berry, B.C., Ebert, B.L., and Fischer, E.S. (2018). Thalidomide promotes degradation of SALL4, a transcription factor implicated in Duane Radial Ray syndrome. Elife *7*, e38430. https://doi.org/10.7554/eLife.38430.

19. Pal, P., Thummuri, D., Lv, D., Liu, X., Zhang, P., Hu, W., Poddar, S.K., Hua, N., Khan, S., Yuan, Y., et al. (2021). Discovery of a Novel BCL-X(L) PROTAC Degrader with Enhanced BCL-2 Inhibition. J. Med. Chem. *64*, 14230–14246. https://doi.org/10.1021/acs.jmedchem.1c00517.

20. Lv, D., Pal, P., Liu, X., Jia, Y., Thummuri, D., Zhang, P., Hu, W., Pei, J., Zhang, Q., Zhou, S., et al. (2021). Development of a BCL-xL and BCL-2 dual degrader with improved anti-leukemic activity. Nat. Commun. *12*, 6896. https://doi.org/10.1038/s41467-021-27210-x.

21. Wang, Z., He, N., Guo, Z., Niu, C., Song, T., Guo, Y., Cao, K., Wang, A., Zhu, J., Zhang, X., and Zhang, Z. (2019). Proteolysis Targeting Chimeras for the Selective Degradation of Mcl-1/Bcl-2 Derived from Nonselective Target Binding Ligands. J. Med. Chem. *62*, 8152–8163. https://doi.org/10.1021/acs.jmedchem.9b00919.

22. Domostegui, A., Nieto-Barrado, L., Perez-Lopez, C., and Mayor-Ruiz, C. (2022). Chasing molecular glue degraders: screening approaches. Chem. Soc. Rev. *51*, 5498–5517. https://doi.org/10.1039/d2cs00197g.

23. Cao, S., Kang, S., Mao, H., Yao, J., Gu, L., and Zheng, N. (2022). Defining molecular glues with a dual-nanobody cannabidiol sensor. Nat. Commun. *13*, 815. https://doi.org/10.1038/s41467-022-28507-1.

24. Soucy, T.A., Smith, P.G., Milhollen, M.A., Berger, A.J., Gavin, J.M., Adhikari, S., Brownell, J.E., Burke, K.E., Cardin, D.P., Critchley, S., et al. (2009). An inhibitor of NEDD8-activating enzyme as a new approach to treat cancer. Nature *458*, 732–736. https://doi.org/10.1038/nature07884.

25. Zhou, J., Dabiri, Y., Gama-Brambila, R.A., Ghafoory, S., Altinbay, M., Mehrabi, A., Golriz, M., Blagojevic, B., Reuter, S., Han, K., et al. (2022). pVHL-mediated SMAD3 degradation suppresses TGF-beta signaling. J. Cell Biol. *221*, e202012097. https://doi.org/10.1083/jcb.202012097.

26. Edison, N., Curtz, Y., Paland, N., Mamriev, D., Chorubczyk, N., Haviv-Reingewertz, T., Kfir, N., Morgenstern, D., Kupervaser, M., Kagan, J., et al. (2017). Degradation of Bcl-2 by XIAP and ARTS Promotes Apoptosis. Cell Rep. *21*, 442–454. https://doi.org/10.1016/j.celrep.2017.09.052.

27. Bai, N., Riching, K.M., Makaju, A., Wu, H., Acker, T.M., Ou, S.C., Zhang, Y., Shen, X., Bulloch, D.N., Rui, H., et al. (2022). Modeling the CRL4A ligase complex to predict target protein ubiquitination induced by cereblon-recruiting PROTACs. J. Biol. Chem. *298*, 101653. https://doi.org/10.1016/j.jbc.2022.101653.

28. Ignatov, M., Jindal, A., Kotelnikov, S., Beglov, D., Posternak, G., Tang, X., Maisonneuve, P., Poda, G., Batey, R.A., Sicheri, F., et al. (2023). High Accuracy Prediction of PROTAC Complex Structures. J. Am. Chem. Soc. *145*, 7123–7135. https://doi.org/10.1021/jacs.2c09387.

29. Bouguenina, H., Nicolaou, S., Le Bihan, Y.V., Bowling, E.A., Calderon, C., Caldwell, J.J., Harrington, B., Hayes, A., McAndrew, P.C., Mitsopoulos, C., et al. (2023). iTAG an optimized IMiD-induced degron for targeted protein degradation in human and murine cells. iScience *26*, 107059. https://doi.org/10.1016/j.isci.2023.107059.

30. Yang, W., Soares, J., Greninger, P., Edelman, E.J., Lightfoot, H., Forbes, S., Bindal, N., Beare, D., Smith, J.A., Thompson, I.R., et al. (2013). Genomics of Drug Sensitivity in Cancer (GDSC): a resource for therapeutic biomarker discovery in cancer cells. Nucleic Acids Res. *41*, D955–D961. https://doi.org/10.1093/nar/gks1111.

31. Dabiri, Y., Kalman, S., Gürth, C.M., Kim, J.Y., Mayer, V., and Cheng, X. (2017). The essential role of TAp73 in bortezomib-induced apoptosis in p53-deficient colorectal cancer cells. Sci. Rep. *7*, 5423. https://doi.org/10.1038/s41598-017-05813-z.

32. Bangi, E., Murgia, C., Teague, A.G.S., Sansom, O.J., and Cagan, R.L. (2016). Functional exploration of colorectal cancer genomes using Drosophila. Nat. Commun. *7*, 13615. https://doi.org/10.1038/ncomms13615.

33. Bangi, E., Ang, C., Smibert, P., Uzilov, A.V., Teague, A.G., Antipin, Y., Chen, R., Hecht, C., Gruszczynski, N., Yon, W.J., et al. (2019). A personalized platform identifies trametinib plus zoledronate for a patient with KRAS-mutant metastatic colorectal cancer. Sci. Adv. *5*, eaav6528. https://doi.org/10.1126/sciadv.aav6528.

34. Zhou, J., and Boutros, M. (2020). JNK-dependent intestinal barrier failure disrupts host-microbe homeostasis during tumorigenesis. Proc. Natl. Acad. Sci. USA *117*, 9401–9412. https://doi.org/10.1073/pnas.1913976117.

35. Zhou, J., Valentini, E., and Boutros, M. (2021). Microenvironmental innate immune signaling and cell mechanical responses promote tumor growth. Dev. Cell *56*, 1884–1899.e5. https://doi.org/10.1016/j.devcel.2021.06.007.

36. Patel, P.H., Dutta, D., and Edgar, B.A. (2015). Niche appropriation by Drosophila intestinal stem cell tumours. Nat. Cell Biol. *17*, 1182–1192. https://doi.org/10.1038/ncb3214.

37. Booy, E.P., Henson, E.S., and Gibson, S.B. (2011). Epidermal growth factor regulates Mcl-1 expression through the MAPK-Elk-1 signalling pathway contributing to cell survival

in breast cancer. Oncogene *30*, 2367–2378. https://doi.org/10.1038/onc.2010.616.

38. Kothari, S., Cizeau, J., McMillan-Ward, E., Israels, S.J., Bailes, M., Ens, K., Kirshenbaum, L.A., and Gibson, S.B. (2003). BNIP3 plays a role in hypoxic cell death in human epithelial cells that is inhibited by growth factors EGF and IGF. Oncogene *22*, 4734–4744. https://doi.org/10.1038/sj.onc.1206666.

39. Mason, K.D., Carpinelli, M.R., Fletcher, J.I., Collinge, J.E., Hilton, A.A., Ellis, S., Kelly, P.N., Ekert, P.G., Metcalf, D., Roberts, A.W., et al. (2007). Programmed anuclear cell death delimits platelet life span. Cell *128*, 1173–1186. https://doi.org/10.1016/j.cell.2007.01.037.

40. Zhang, H., Nimmer, P.M., Tahir, S.K., Chen, J., Fryer, R.M., Hahn, K.R., Iciek, L.A., Morgan, S.J., Nasarre, M.C., Nelson, R., et al. (2007). Bcl-2 family proteins are essential for platelet survival. Cell Death Differ. *14*, 943–951. https://doi.org/10.1038/sj.cdd.4402081.

41. Roberts, A.W., Davids, M.S., Pagel, J.M., Kahl, B.S., Puvvada, S.D., Gerecitano, J.F., Kipps, T.J., Anderson, M.A., Brown, J.R., Gressick, L., et al. (2016). Targeting BCL2 with Venetoclax in Relapsed Chronic Lymphocytic Leukemia. N. Engl. J. Med. *374*, 311–322. https://doi.org/10.1056/NEJMoa1513257.

42. Seymour, J.F., Ma, S., Brander, D.M., Choi, M.Y., Barrientos, J., Davids, M.S., Anderson, M.A., Beaven, A.W., Rosen, S.T., Tam, C.S., et al. (2017). Venetoclax plus rituximab in relapsed or refractory chronic lymphocytic leukaemia: a phase 1b study. Lancet Oncol. *18*, 230–240. https://doi.org/10.1016/S1470-2045(17)30012-8.

43. Fresquet, V., Rieger, M., Carolis, C., García-Barchino, M.J., and Martinez-Climent, J.A. (2014). Acquired mutations in BCL2 family proteins conferring resistance to the BH3 mimetic ABT-199 in lymphoma. Blood *123*, 4111–4119. https://doi.org/10.1182/blood-2014-03-560284.

44. Blombery, P., Anderson, M.A., Gong, J.N., Thijssen, R., Birkinshaw, R.W., Thompson, E.R., Teh, C.E., Nguyen, T., Xu, Z., Flensburg, C., et al. (2019). Acquisition of the Recurrent Gly101Val Mutation in BCL2 Confers Resistance to Venetoclax in Patients with Progressive Chronic Lymphocytic Leukemia. Cancer Discov. *9*, 342–353. https://doi.org/10.1158/2159-8290.Cd-18-1119.

45. Schapira, M., Calabrese, M.F., Bullock, A.N., and Crews, C.M. (2019). Targeted protein degradation: expanding the toolbox. Nat. Rev. Drug Discov. *18*, 949–963. https://doi.org/10.1038/s41573-019-0047-y.

46. Posternak, G., Tang, X., Maisonneuve, P., Jin, T., Lavoie, H., Daou, S., Orlicky, S., Goullet de Rugy, T., Caldwell, L., Chan, K., et al. (2020). Functional characterization of a PROTAC directed against BRAF mutant V600E. Nat. Chem. Biol. *16*, 1170–1178. https://doi.org/10.1038/s41589-020-0609-7.

47. Chen, L., and Bourguignon, L.Y.W. (2014). Hyaluronan-CD44 interaction promotes c-Jun signaling and miRNA21 expression leading to Bcl-2 expression and chemoresistance in breast cancer cells. Mol. Cancer *13*, 52. https://doi.org/10.1186/1476-4598-13-52.

48. Kang, H., Hasselbeck, S., Taškova, K., Wang, N., Oosten, L.N.V., Mrowka, R., Utikal, J., Andrade-Navarro, M.A., Wang, J., Wölfl, S., and Cheng, X. (2023). Development of a next-generation endogenous OCT4 inducer and its anti-aging effect in vivo. Eur. J. Med. Chem. *257*, 115513. https://doi.org/10.1016/j.ejmech.2023.115513.

49. Schwalm, M.P., Krämer, A., Dölle, A., Weckesser, J., Yu, X., Jin, J., Saxena, K., and Knapp, S. (2023). Tracking the PROTAC degradation pathway in living cells highlights the importance of ternary complex measurement for PROTAC optimization. Cell Chem. Biol. *30*, 753–765.e8. https://doi.org/10.1016/j.chembiol.2023.06.002.